REPORT DOCUMENTATION PAGE

AFRL-SR-BL-TR-00-

0634

1. AGENCY USE ONLY *(Leave blank)*	2. REPORT DATE	15 April 1996 - 14 April 1998

4. TITLE AND SUBTITLE
Statistical Modeling and Simulation for Microstructure in Materials Science

5. FUNDING NUMBERS
F49620-96-1-0133

6. AUTHOR(S)
Chuanshu JI

7. PERFORMING ORGANIZATION NAME(S) AND ADDRESS(ES)
University of North Carolina
Department of Statistics
Chapel Hill, NC 27599-3260

8. PERFORMING ORGANIZATION REPORT NUMBER

9. SPONSORING/MONITORING AGENCY NAME(S) AND ADDRESS(ES)
AFOSR
801 North Randolph Street, Room 732
Arlington, VA 22203-1977

10. SPONSORING/MONITORING AGENCY REPORT NUMBER
F49620-96-1-0133

11. SUPPLEMENTARY NOTES

12a. DISTRIBUTION AVAILABILITY STATEMENT
Approved for Public Release.

12b. DISTRIBUTION CODE

13. ABSTRACT *(Maximum 200 words)*

The main accomplishment in this project consists of two parts: (I) Reconstruction cycle in microstructure modeling; and (II) Computation of effective properties via Markov chain Monte Carlo (MCMC) algorithms. The details are contained in Derr (1998) -- a draft of Ph.D. dissertation entitled "Statistical modeling of microstructure with applications to effective property computation in materials science" by Bob Derr under the supervision of Chuanshu Ji. One of the most important issues in materials science is the connection between materials prop-erties, e.g. conductivity, elastic moduli, strength, etc. and microstructures. Along this line, many computer models were proposed to generate synthetic microstructures on which some numerical schemes, e.g. finite element, were used to calculate the materials properties of interest, assuming the local properties satisfy certain partial differential equations for stress/strain or diffusions. On the other hand, experimentation was conducted in laboratories which measures those properties from real materials. A significant gap exists between these two aspects of the study due to the lack of methodology for fitting the computer models (i.e. estimating the parameters in those models) based on the real microstructure data.

20001127 022

14. SUBJECT TERMS			15. NUMBER OF PAGES 11
			16. PRICE CODE
17. SECURITY CLASSIFICATION OF REPORT	18. SECURITY CLASSIFICATION OF THIS PAGE	19. SECURITY CLASSIFICATION OF ABSTRACT	20. LIMITATION OF ABSTRACT

FINAL REPORT

Project Identification: AFOSR Grant F49620-96-1-0133
Project Title: Statistical Modelling and Simulation for Microstructure in Materials Science
Principal Investigator: Chuanshu Ji, UNC-Chapel Hill, cji@stat.unc.edu

The main accomplishment in this project consists of two parts: (I) Reconstruction cycle in microstructure modelling; and (II) Computation of effective properties via Markov chain Monte Carlo (MCMC) algorithms.

The details are contained in Derr (1998) — a draft of Ph.D. dissertation entitled "Statistical modelling of microstructure with applications to effective property computation in materials science" by Bob Derr under the supervision of Chuanshu Ji. Several papers based on this thesis are being written and to be sumitted for publication.

I. Reconstruction cycle in microstructure modelling

One of the most important issues in materials science is the connection between materials properties, e.g. conductivity, elastic moduli, strength, etc. and microstructures. Along this line, many computer models were proposed to generate synthetic microstructures on which some numerical schemes, e.g. finite element, were used to calculate the materials properties of interest, assuming the local properties satisfy certain partial differential equations for stress/strain or diffusions. On the other hand, experimentation was conducted in laboratories which measures those properties from real materials. A significant gap exists between these two aspects of the study due to the lack of methodology for fitting the computer models (i.e. estimating the parameters in those models) based on the real microstructure data.

Several steps were taken in this project towards bridging such a gap. A class of statistical models for microstructure — hard-core/soft-shell elliptical processes, simply called elliptical processes, was proposed, and the related modelling task was carried out via the following reconstruction cycle:

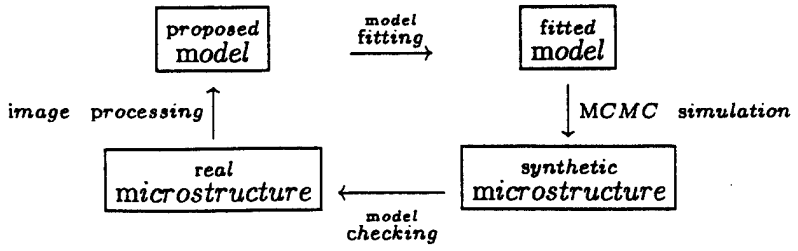

Step 1. Descriptive data summary: microstructure image processing;

Step 2. Model fitting: parameter estimation in the proposed probability density;

Step 3. Simulation from the fitted model: Markov chain Monte Carlo (MCMC) algorithms;

Step 4. Model checking: good of fit tests, comparisons of features.

Although this follows from the basic principle in statistical modelling, its implementation on models as complex as the elliptical processes is new and challenging. The main consideration in choosing this model class is the combination of practicality and feasibility. The hard-core assumption is essential in modelling microstructure since particles (grains) in 3D are nonoverlapping. The main technical difficulty with the hard-core assumption lies in that it induces complicated spatial dependence structures. The class of elliptical processes has several advantages. On one hand, it is rich enough to generate a great variety of synthetic microstructural patterns (see Fig. 1c, 1d, 2a – 2f), because it allows variability in location, orientation, aspect ratio and size of ellipses. On the other hand, it is computationally manageable (although intensive), since it is still a finite-dimensional model (the dimensionality can be quite high). More realistic microstructures and flexible deformable shapes can be approximated when computational facilities permit. Although this report only summarizes results for the 2D elliptical processes, the extension to 3D ellipsoidal processes can be handled in a similar manner.

Step 1. Take the real microstructures in Fig. 1a and 1b, approximate them by nonoverlapping ellipses via range-oriented fitting or least-squares fitting [cf. Derr (1998)].

Step 2. A configuration $x = \{x_1, \ldots, x_n\}$ consists n ellipses, each denoted by $x_i = (\xi_i, \theta_i, a_i, b_i)$, with center ξ_i, orientation θ_i, major and minor half-axes a_i and b_i respectively. The probability distribution of an elliptical process is characterized by its density $f(x)$ with respect to a reference measure $\mu \times \nu$. Under μ, $\{\xi_i\}$ form a homogeneous Poisson process in a bounded region $S \subset \mathbb{R}^2$ with the mean measure being the area $m(S)$ of S, and under ν, $\{(\theta_i, a_i, b_i)\}$ are iid marks with θ_i uniformly distributed on $[0, \pi]$, and (a_i, b_i) uniformly distributed over the triangle $\{l \le b_i \le a_i \le L\}$, where $l < L$ are two known positive constants, to be specified in the experiment.

The density $f(x)$ has a form

$$f(x; \lambda, a, b) = \lambda^n h(x; a, b)[B(\lambda, a, b)]^{-1},$$

with

(1)

$$h(x; a, b) = I_{(b \le b_{n1} \le a_{nn} \le a)} A(x) \prod_{i=1}^{n} g(x_i),$$

where

(i) $a_{nn} = \max_{1 \le i \le n} a_i$, and $b_{n1} = \min_{1 \le i \le n} b_i$ [in general, a_{ni} denotes the ith order statistics in $(a_1, \ldots, a_n)$], and I_A is the indicator function of an event A;

(ii) λ, a and b are three unknown parameters, with the assumed ranges $\lambda > 0$ and $l \le b \le a \le L$, and the sufficient statistics $\{n, a_{nn}, b_{n1}\}$;

(iii) $g(x_i) > 0$ $\forall x_i$ and $\forall i$, with a known function g, depends on x_i only through its area, e.g. $g(x_i) = 1$, or $g(x_i) = a_i b_i$, or $g(x_i) = (a_i b_i)^{-1}$, to give a few particular choices;
(iv) The factor $A(x) \geq 0$ $\forall x$ includes the range restriction $0 \leq \theta_i \leq \pi$, $a_i \geq b_i$ $\forall i$, and the nonovelapping restriction, etc., but does not involve the unknown parameters;
(v) The normalization factor is expressed as

$$B(\lambda, a, b) = \sum_k \{e^{-m(S)}[m(S)]^k/k!\} \int_{S^k} \int_{[0,\pi]^k} \int_{[b,a]^{2k}} \lambda^k h(x; a, b) \prod_{i=1}^{k} (d\xi_i d\theta_i da_i db_i), \tag{2}$$

with the term $e^{-m(S)}$ when $k = 0$. Note that $B(\lambda, a, b)$ is practically a finite sum. Since every ellipse has a minor half-axis no less than $l > 0$, and the ellipses are nonoverlapping with their centers distributed over the bounded region S, any configuration consists only a finite number of such ellipses.

Denote the maximum likelihood estimates (MLE) for λ, a and b by $\hat{\lambda}$, $\hat{a}$ and $\hat{b}$ respectively. Then

$$\hat{a} = a_{nn} \quad \text{and} \quad \hat{b} = b_{n1}. \tag{3}$$

The MLE $\hat{\lambda}$ can be found by solving the equation

$$\lambda \frac{d}{d\lambda} B(\lambda, a_{nn}, b_{n1}) - nB(\lambda, a_{nn}, b_{n1}) = 0, \tag{4}$$

using Monte Carlo approximate likelihood [cf. Derr (1998)]. Alternatively, the ratio $\frac{n}{m(S)}$ appears to be a simple reasonable estimate of λ.

Step 3. To simulate spatial patterns from a target distribution defined on a large configuration space Ω, the basic idea of MCMC is to construct a Markov process $X = \{X_t\}$ such that it has the target distribution as its (unique) equilibrium distribution. The key is to incorporate the knowledge of the target distribution into the transition probability mechanism of X. A special case of MCMC — spatial birth-and-death processes (SBDP) — is suitable for simulation of the elliptic processes. A sufficient (reversibility) condition to guarantee the convergence to the equilibrium density f, with a birth rate $b(\cdot)$ and a death rate $D(\cdot)$, is the following detailed balance equation

$$f(x^n)\ b(x^n, x_{n+1}) = f(x^{n+1})\ D(x^n, x_{n+1}) \quad \text{whenever} \quad f(x^{n+1}) > 0, \tag{5}$$

where the notation $x^n = \{x_1, \ldots, x_n\}$ indicates the number of objects in x, and the dependence of f on parameters [as shown in (1)] is suppressed.

Even with the knowledge of a fully specified f in (5), there are still many different choices for $b(\cdot)$ and $D(\cdot)$. One is to specify

$$D(x^n, x_{n+1}) = 1/g(x_{n+1}), \tag{6}$$

thus the birth rate accordingly by (5),

$$b(x^n, x_{n+1}) = D(x^n, x_{n+1})\ f(x^{n+1})/f(x^n)$$
$$= \begin{cases} \lambda, & \text{if } x_{n+1} \text{ does not overlap } x_i\ \forall i = 1, \ldots, n, \\ 0, & \text{otherwise.} \end{cases} \tag{7}$$

This can be easily implemented.

Step 4. Checking whether data fit a proposed model can be done either in the parameter space or in the sample space. For the problem considered in this work, the MLEs were derived which enjoy many good asymptotic properties; but comparisons in the sample space might be more meaningful since one really wants to "see" if the synthetic microstructures resemble the real ones. The sample space of microstructural images has high dimensionality. Some average-based norms such as L^2-norm, etc. often fail to highlight the difference in certain particular features which may be more relevant to the underlying materials. Hausdorff metric for shape comparison could be used but instead, some simple feature extraction was used in this project. For each of the features (location, orientation, aspect ratio and size), two histograms were plotted, one for the original microstructure image, one for the synthetic one generated from the fitted model [cf. Derr (1998)]. Some goodness of fit tests were conducted to compare the empirical distributions.

Notice that there are many other mothods in materials science literature to generate synthetic microstructures, but they suffer from a common drawback — lack of reconstruction capability, because they are not tuned to real microstructures. The approach taken in this project is expected to make a notable impact to this area.

II. Computation of effective conductivity via Markov chain Monte Carlo

The great variability of local properties in heterogeneous materials makes the computation of global properties an important and challenging project. The result obtained in this project concerns computation of effective conductivity using MCMC. The approach looks promising and should work for computation of effective elastic moduli as well.

The approach was originally introduced by in Brown (1955) and then extended in a number of papers by Torquato et al. This approach demonstrates explicitly the connection between the effective conductivity and the statistical distribution of microstructural features, in particular the k-point probability functions ($k = 1, 2, \ldots$), hence it is capable of handling multiple representations in different length scales. It becomes quite clear that the promise of this approach relies on some ingenious computational techniques.

For the simple illustration purpose, consider a two-phase composite material represented by the 2D domain S and follow the notation in Part I. The phase i itself is homogeneous with constant electrical conductivity $\sigma_i > 0$, $i = 1, 2$. Assume the phase 1 region, $R_1 \subset S$, is precisely covered by the configuration x with n nonoverlapping grains (e.g. ellipses), and $R_2 = S \backslash R_1$ is the phase 2

region. Define the local conductivity

$$\sigma(z) = \sigma_1 I_{\{z \in R_1\}} + \sigma_2 I_{\{z \in R_2\}}, \quad z \in S. \tag{8}$$

Hence $\sigma(z)$, $z \in S$ is a random field resulting from the random distribution of x.

Materials scientists are interested in the effective behavior of heterogeneous media. In this setting, *if* there is a homogeneous medium, the effective medium S^*, whose conductivity σ^* is close to the conductivity of S when measured on a large space scale, then σ^* is called the effective conductivity.

There are two issues. The first one is to justify the exitence of σ^* — the averaging, called homogenization, takes place so that the complex small scale random structure is replaced by an asymptotically equivalent homogeneous deterministic structure. Papanicolaou (1995) is an excellent survey for the related homogenization theory.

The second issue, computation of σ^*, is practically more relevant in materials science. Following the perturbation expansion approach originally developed by Brown (1955), Torquato and his collaborators made significant contributions to this problem [cf. Torquato (1985), Sen and Torquato (1989), Torquato and Sen (1990), and Torquato (1991)]. The perturbation expansion for d-dimensional media (in particular, $d = 2$ or 3) given in these papers is expressed as

$$(q_i\beta_{ij})^2(\sigma^* - \sigma_j \cup)^{-1}[\sigma^* + (d-1)\sigma_j \cup] \;=\; q_i\beta_{ij} \cup - \sum_{k=2}^{\infty} A_k^{(i)} \beta_{ij}^k, \qquad i \neq j,\ i,j = 1,2, \tag{11}$$

where the tensor coefficients $A_k^{(i)}$ are represented as integrals:
for $k = 2$,

$$A_2^{(i)} \;=\; \frac{d}{2\pi(d-1)} \int_\delta T_{12} \cdot (P_{1,2}^i - q_i^2)\, dz_2, \tag{12}$$

where the subscript δ on the integral indicates that it is carried out with the exclusion of an infinitesimal neighborhood of z_1 (i.e. a tiny d-dimensional sphere centered at z_1);
and for $k \geq 3$,

$$A_k^{(i)} \;=\; (-1)^k q_i^{2-k} \left[\frac{d}{2\pi(d-1)}\right]^{k-1} \int \cdots \int (T_{12} \cdots T_{k-1,k} \cdot D_k^i)\, dz_2 \cdots dz_k. \tag{13}$$

The notation in (11), (12) and (13):

- q_i is the volume (area) fraction of phase i;
- $\beta_{ij} = \frac{\sigma_i - \sigma_j}{\sigma_i + (d-1)\sigma_j}$;
- Each $z_m \in S$, as a d-dimensional column vector, has norm $|z_m|$, $m = 1, \ldots, k$;
- $T_{m-1,m} \;=\; |z_m - z_{m-1}|^{-d-2}[\; d\; (z_m - z_{m-1})(z_m - z_{m-1})^t - |z_m - z_{m-1}|^2 \cup\;]$ is the dipole-dipole interaction tensor, where z^t represents the transpose of z (thus a row vector), and $\cup$ the unit dyadic [see Nemat-Nasser and Hori (1993) Section 15 for the basic tensor notation and terms], (the integrand $T_{12} \cdots T_{k-1,k} \cdot D_k^i$ is a function of $z_1, \ldots, z_k$);

For the determinant

$$D_k^i = \begin{vmatrix} P_{1,2}^i & P_{2,2}^i & 0 & \cdots & 0 & 0 \\ P_{1,3}^i & P_{2,3}^i & P_{3,3}^i & \cdots & 0 & 0 \\ & & \cdots & \cdots & & \\ P_{1,k-1}^i & P_{2,k-1}^i & P_{3,k-1}^i & \cdots & P_{k-2,k-1}^i & P_{k-1,k-1}^i \\ P_{1,k}^i & P_{2,k}^i & P_{3,k}^i & \cdots & P_{k-2,k}^i & P_{k-1,k}^i \end{vmatrix}, \tag{14}$$

its entry P_{m_1,m_2}^i is the probability that all $(m_2 - m_1 + 1)$ points $z_{m_1}, z_{m_1+1}, \ldots, z_{m_2}$ are contained in the phase i region R_i, where $m_1, m_2 = 1, \ldots, k$ and $m_1 \leq m_2$.

Numerical computation of $A_k^{(i)}$ is crucial and intensive, especially for large k. Most of the previous works were limited to the derivation of lower-order bounds (for $k \leq 5$). These bounds provided useful approximations of the conductivity for certain special cases of microstructure, but the result in the related error estimate was lacking and the gap between the available bounds and the true value of conductivity remained large in many situations. Therefore, the need for solving the long-standing open problem of deriving higher-order approximations ($k > 5$) of $A_k^{(i)}$ for a variety of microstructures became more urgent. In this regard, this work has made good progress in:

(i) estimating the k-point probability function $P_{1,k}^i$ for a wide range of $z_1, \ldots, z_k$, based on MCMC simulation;

(ii) developing some recursive formulas to reduce the k-point probability function to a sequence of two-point probability functions, thus the computational speed is significantly improved [cf. Derr (1998)];

(iii) calculating the high-dimensional multiple integral involved in $A_k^{(i)}$ by Monte Carlo methods.

Plasma-sprayed coating

Plasma-sprayed coating (see Fig. 3a and 3b) is an important application in which the relationship between microstructure and properties can be studied. The approach developed in this project appears promising for the quatitative study of coating microstructures and computation of thermal conductivity. Only partial results are available right now. This is still a part of ongoing research.

In aircraft engines plasma-sprayed metallic coatings protect turbine blades from highly corrosive environments, and plasma-sprayed ceramics insulate other engine parts from high temperatures [cf. Herman (1988)]. The powdered coating material, carried in a stream of gas such as argon, is injected into the jet of plasma from a plasma gun. The flame accelerates the particles, and they are melted by its high temperature. The molten droplets are propelled onto the target surface, where they solidify and accumulate to form a thick, tenaciously bonded protective coating. Particles continue to rain down at a rate that depends on the area to be covered and how fast the gun moves over the surface.

Transmission electron microscopy helps examine the internal structure of particles and coatings; scanning electron microscopy reveals overall shapes and textures. The internal structure — a mosaic of crystalline grains — contains many flaws, suggesting that each particle solidifies extremely quickly, in perhaps a millionth of a second. Ceramic coatings in particular reveal a multitude of flaws. They are riddled with cracks formed as the ceramic cooled and are honeycombed with voids filled with air trapped in the deposit. Such flaws can doom a coating exposed to mechanical stress. If they extend all the way through the coating, they also make it useless for protection against corrosion.

Strangely, it is porosity that suits plasma-sprayed ceramic coatings to one of their most important applications: as thermal-barrier coatings, which are insulating coatings for metal parts exposed to very high temperatures in gas turbines and other kinds of engines. For one thing, porosity increases a ceramic's insulating ability. Moreover, porosity and microcracks could enhance strain tolerance. This is because a ceramic is brittle in the first place, pores do not weaken the material but instead toughen it by interrupting the propagation of the cracks that inevitably form as the material is strained. By retaining lubricants, pores also benefit some plasma-sprayed coatings designed to protect against wear. There is trade-off, however, that such voids could be fatal to many wear-resistant metallic coatings and coatings meant to prevent their substrate from corroding or oxidizing. Some multi-layered coatings are used now in which vacuum plasma spraying yields a dense, void-free metallic coating, followed by ceramic thermal-barrier coatings.

To control the degree of porosity in different coatings when processing the materials, an important step is the quantification of porosity. Fig. 3a and 3b show the complex porosity distribution. The empirical estimate of porosity was obtained via image processing. Extensive lab experiments were conducted at NIST. However, modelling the coating microstructure appears very difficult. A starting point is to use a similar models to Fig. 2c to simulate the fibre process in which nearly horizontal fibres imitate gaps between coating particles, while nearly vertical fibres may represent microcracks. Then the horizontal and vertical components of the effective thermal conductivity tensor can be calculated using the method in Part II. The numerical calculation can be compared with the results of lab tests in the study of such coatings as a thermal barrier. Similar studies in calculation of mechanical properties of coatings will be pursued also.

References

(1) Brown, W.F.J. (1955). Solid mixture permittivities. *J. Chem. Phys.* **23**, 1514-1517.

(2) Derr, R.E. (1998). *Statistical Modelling of Microstructure with Applications to Effective Property Computation in Materials Science.* Ph.D. dissertation (under the supervision of Chuanshu Ji).

(3) Geary, A.R. (1980). Evaluation of thermal sprayed coatings. *Microstructural Science* **19**, 637-650.

(4) Herman, H. (1988). Plasma-sprayed coatings. *Scientific American* (Sept.), 112-117.

(5) Nemat-Nasser, S. and Hori, M. (1993). *Micromechanics: Overall Properties of Heterogeneous Materials.* Elsevier Science, Amsterdam, The Netherlands.

(6) Papanicolaou, G.C. (1995). Diffusion in random media. *Surveys in Applied Mathematics*, Keller, J.P. (ed.) **1**, 205-253. Plenum Press, New York.
(7) Sen, A.K. and Torquato, S. (1989). Effective conductivity of anisotropic two-phase composite media. *Physical Review B 39*, 4504-4515.
(8) Torquato, S. (1985). Effective electrical conductivity of two-phase disordered composite media. *J. Appl. Phys.* **58**, 3790-3797.
(9) Torquato, S. (1991). Random heterogeneous media: microstructure and improved bounds on effective properties. *Appl. Mech. Rev.* **44**, 37-76.

Interdisciplinary activity and Ph.D. supervision

The P.I. was invited to give talks related to this project in a number of statistics colloquia (at various Statistics Departments), and also at the following materials science conferences:
• IMM Workshop on Rational Design and Processing of Advanced Ceramics, June 21-23, 1995, La Jolla, CA;
• IEEE 1995 International Conference on Image Processing, October 23-26, 1995, Washington, D.C.;
• 7th ACBM/NIST Computer Modelling Workshop, 8/4/96-8/11/96, Gaithersburg, MD.;
• 5th Annual Meeting of Young Investigators on Mechanical Properties of Materials and Reliability Issues, August 1997, GE Research Center, Schenectady, NY.

Other than the P.I. (Chuanshu Ji), the following individuals were supported by the AFOSR grant when they, as Ph.D. students under the supervision of Chuanshu Ji, participated in the proposed research.
• Aluisio Pinheiro: male, citizen of Brazil, Ph.D. (1997), now at Cidade University, Brazil;
• Robert Edwin Derr: male, U.S. citizen, Ph.D. (1998, expected), now at SAS Institute;
• Xin Ge: male, citizen of P.R. China, Ph.D. candidate at UNC-Chapel Hill.

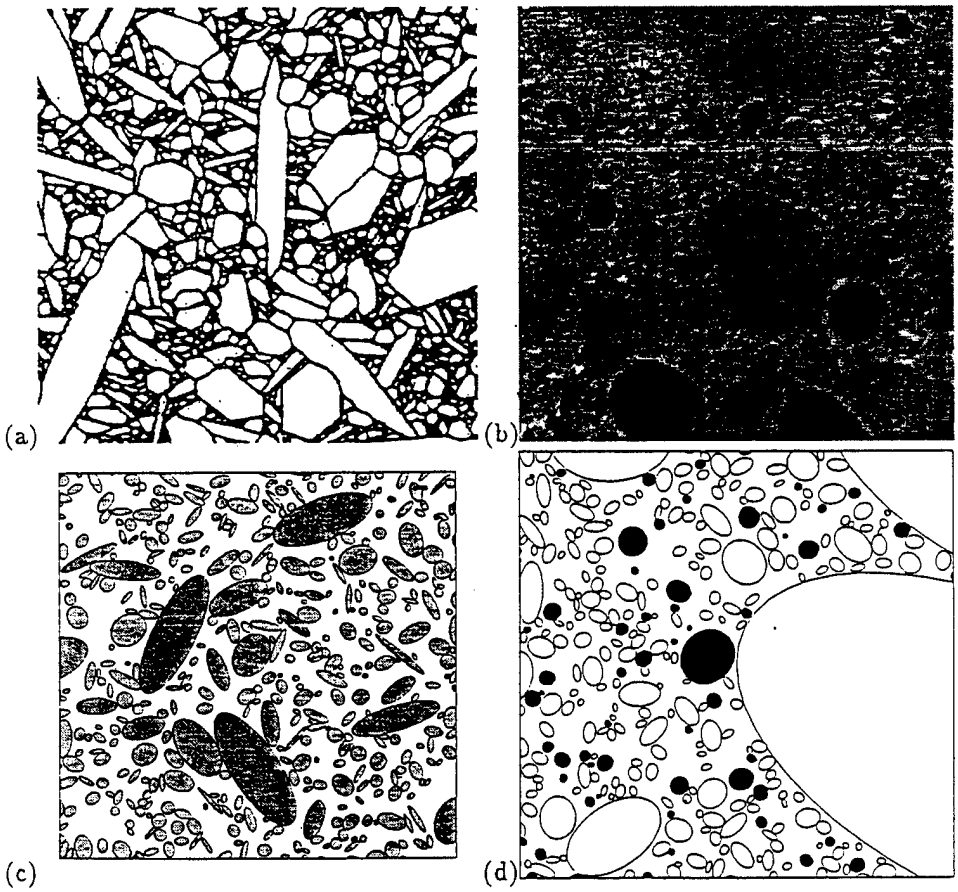

Figure 1: (a) (Processed) SEM image of in-situ toughened Si_3N_4 ceramic crystals grown in a sintering process. (b) Mortar (concrete) — sands mixed in a cement paste: the large irregular grains are sands; the smaller circular particles are bubbles or pores; the laminate is a concrete mixture; and there is a narrow *interfacial zone* between the rocks which keeps two rocks from actually touching. (c) Synthetic microstructure simulated from an elliptical process fitted by the Si_3N_4 image data (a). (d) Synthetic microstructure simulated from a mordified elliptical process fitted by the mortar image data (b). The modification involves coding all ellipses into two different types, in which the sands are outlined while the pores are filled in black.

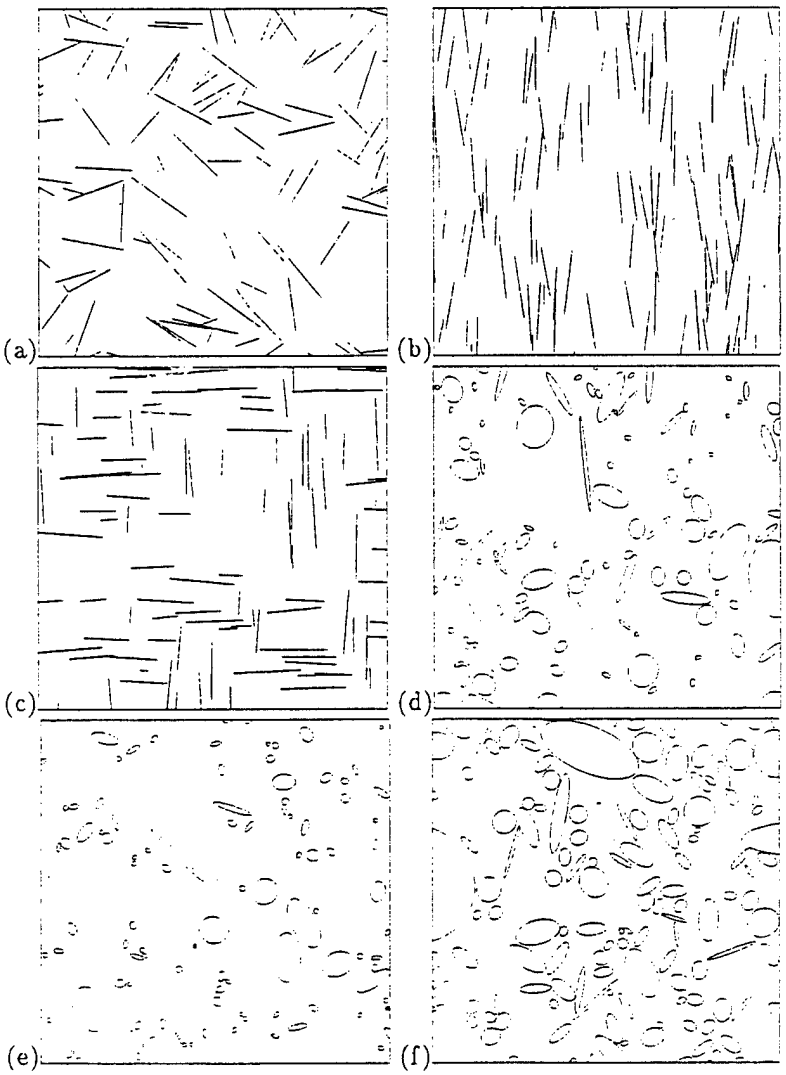

Figure 2: The fibres (line segments) in (a), (b) and (c) are actually narrow ellipses (aspect ratio 0.005) with lengths uniformly distributed in $[0.01, 0.1]$: (a) randomly oriented fibres; (b) fibre orientation constrained to be within $\pi/8$ of the vertical; (c) fibre orientation constrained within $\pi/16$ of the vertical or horizontal. The ellipses in (d), (e) and (f) are samples of SBDP using different forms of $g(\cdot)$ in the death rate (6): (d) constant $g(\cdot)$; (e) $g(\cdot)$ inversely proportional to the size of the ellipses: (f) $g(\cdot)$ proportional to the size of the ellipses.

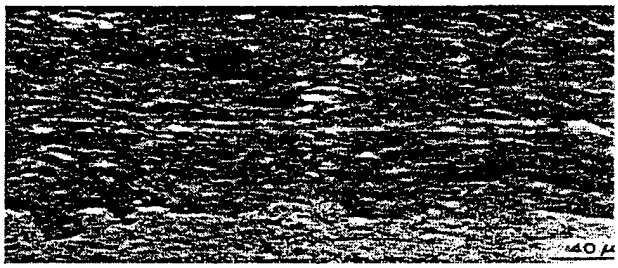

(a)

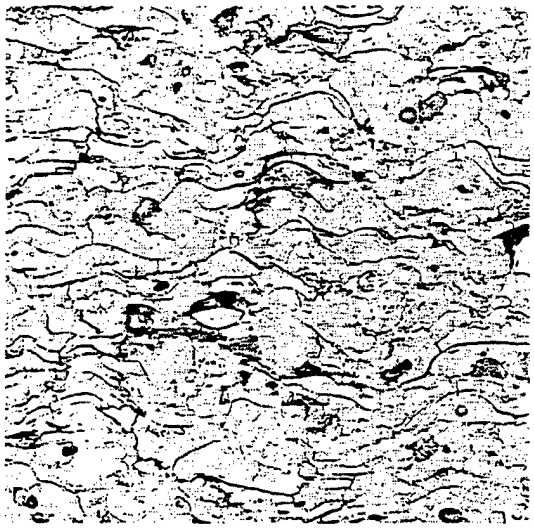

(b)

Figure 3: (a) is taken from Geary (1980) which shows the microstructure of an aluminum-oxide coating (the upper thick dark layer) over a nickel-aluminum bond coating (the lower thin light layer). (b) is a microstructure (with width 50 μm) of Zirconia ZrO_2 coating.